Case Studies in Engineering Failure Analysis 4 (2015) 39–49

Contents lists available at ScienceDirect

Case Studies in Engineering Failure Analysis

journal homepage: www.elsevier.com/locate/csefa

Case study

Perforated mechanism of a water line outlet tee pipe for an oil well drilling rig

Peng Cheng-hong*, Zhu Wei-heng, Liu Zheng-yi, Wei Xing-zhao

School of Materials Science and Engineering, South China University of Technology, Guangzhou 510641, China

ARTICLE INFO

Article history:
Received 9 March 2015
Received in revised form 14 July 2015
Accepted 22 July 2015
Available online 31 July 2015

Keywords:
Tee pipe
Cavitation erosion
Twin crystal
Electrochemical corrosion

ABSTRACT

A corroded tee pipe belonging to a 10-in new separator water line outlet installed in an offshore oil well drilling rig was investigated. The configuration of the large corroded pit had the shape of an imperfect horse's hoof with a completely corroded interior and a honeycomb-like cavity. There is a badly corroded pit at the welded seam at the joint connecting the tee pipe and flange. The material strength of the tee pipe meets the requirement of ASTM-A234 Gr. WPR, but its chemical composition does not meet the stipulated requirements. A deformed streamline structure or twin crystal in the ferrite phase can be seen near the surface or sub-surface of the perforated corrosion puncture edge. The micro-hardness is also different from that of the original material. The SEM results show that the puncture appears to have been a mode of quasi-cleavage fractures with secondary cracks along the direction of the crystal grain; thus, the failure has the features of mechanical and chemical corrosion. The corroded surface contains high amounts of O, C, and N, as well as S, Cl, Si, Na, Mg, Al, K, Ti, etc., all of which are corrosion products caused by sea water. The penetrating puncture hole at the turn of the tee pipe is likely the result of cavitation erosion accompanied by chemical/electrochemical corrosion, and the corrosion on the seam connecting the tee pipe and flange is likely the result of electrochemical corrosion.

1. Introduction

Corrosion in oil drilling and transport pipelines is very common [1–7]. The perforated pipe examined in this study is a tee pipe, which is a 10-in new separator water line outlet installed on an offshore oil well-drilling rig, as shown in Fig. 1, where Fig. 1(a) shows its exterior, Fig. 1(b) shows its interior and Fig. 1(c) and (d) shows its corroded areas.

The tested tee pipe was installed on an offshore oil well-drilling rig, and the fluid flowing in the pipe was the oil-containing sewage produced after crude oil has been separated. The pipe was perforated due to corrosion after only 6–12 months of use. The perforation in the pipe is a small-size hole near the pipe joint corner and has a simple shape (arrow 1); the corroded area, however, is relatively large (arrow 2).

* Corresponding author. Tel.: +86 20 22236389; fax: +86 20 87111317.
E-mail address: mehpeng@scut.edu.cn (C.-h. Peng).

http://dx.doi.org/10.1016/j.csefa.2015.07.002

Fig. 1. Interior and exterior of the perforated tee pipe. (a) Exterior; (b) interior; (c) interior of the corroded cavity; (d) interior of location "3" in Fig. 1 (b).

The tee pipe is made of ASTM A234 steel, and the joint flange is made of ASTM A105 steel.
Failure analyses of the perforated failed tee pipe were performed to determine the cause of its failure.

2. Experimental procedure

Based on the analysis requirements and the consignor's demands, test samples were taken from the area around the corroded puncture and from the area where there was no apparent corrosion. The following aspects of the samples were analyzed: metallurgical structure, EM scanning, chemical composition, and mechanical properties (e.g., tension). Chemical composition tests of the materials used to make the tee pipe and joint flange are performed via a photoelectric direct-reading spectrometer DV6E.

All metallographic grinding surfaces were etched by 4% nitric acid-alcohol-mixed liquid to allow observation of their metallographic microstructure. The specimens' microstructures were investigated using optical microscopy (Leica, Germany). The puncture surfaces were ultrasonically cleaned and observed with a scanning electron microscope (SEM, Shimadzu, EPMA1600, Japan) equipped with energy-dispersive X-ray spectroscopy (EDX). The microhardnesses of the pit edge zones and matrix were measured using a Vickers microhardness tester. To confirm the failure mechanism, the corrosion products at the perforation were analyzed by a scanning electron microscope equipped with EDX.

Table 1
Material strength test of the tee pipe.

Performance indices	σ_s (MPa)	σ_b (MPa)	δ (%)
Tee pipe	324	496	34.8
ASTM-A234 Gr. WPR [11]	315	435–610	20
Joint flange	The corroded part of the flange to be test is too small to be sampled.		

3. Results

3.1. Interior and exterior of the perforated tee pipe

The configuration of the large corroded pit (arrow 2 in Fig. 1(b)) has the shape of an imperfect horse's hoof, as shown in Fig. 1(c). The surface of the pipe (arrow 3) does not seem to be corroded based on its outward appearance; however, but its interior is completely corroded and forms a honeycomb-like cavity, as shown in Fig. 1(d). The large corroded pit seems to be a funnel-shaped basin formed by corrosion which began from the inner surface of the pipe and extended in two direction; in one direction, axial extension that extends the range of the corrosion is shown; in the another direction, radial extension that deepens the corroded cavity and forms a pocket, whose bottom is perforated and whose walls are covered with many small corroded basin, is shown. All corroded basins have similar shapes, their arrangements are regular, and their images look like hillside terraced fields that have a field ridge, dull colors, the capability of reflecting light and are not covered with corroded substances.

It can be seen from Fig. 1(b) that there is another large corroded pit in the pipe wall in addition to the perforated pit, as indicated by arrow 4 in Fig. 1(c).

A badly corroded pit at the welded seam is also present; this seam is located at the joint connecting the tee pipe and the flange, as indicated by arrow 5.

On the inner surface of the tee pipe, there is a light smooth orange paint coat in addition to the corroded area.

From the appearance of the corroded pit, there are characteristics of cavitation erosion and turbulence erosion [8–10].

3.2. Analysis of samples

3.2.1. Test of strength

As shown in Fig. 1(b), axial specimens with round sections were taken from the area that shows no corrosion. The results are listed in Table 1.

3.2.2. Tests of chemical compositions

Using tensile tests, the chemical composition tests of the steel (i.e., the orange paint coat taken from the inner surface of the corroded pipe) are performed; the test results are shown in Table 2.

As shown from the general chemical composition of materials (i.e., the element category and mass percentage and compared with the chemical compositions of standard steels stipulated by grade WPR of Series 234 of the American standard ASTM), the contents of C in the tee pipe are similar to the standard; the contents of Mn are marginally higher than the standard; Ni and Cu of the tee pipe is respectively a little higher and much lower than the standard. Considering the steels used in the corroded media, the content of Cu is important, and thus, it is reasonable to conclude that the chemical composition of the tee pipe do not meet the requirements of the standard steel chemical compositions stipulated in grade WPR of Series 234 of the American standard ASTM.

Conversely, the chemical composition of the flange meets the requirements of the standard steel chemical compositions stipulated in A 105 of the American standard ASTM.

Table 2
Chemical composition of the tee pipe.

Materials	Chemical compositions (mass percentage %)										
	C	Si	Mn	P	S	Cr	Ni	Cu	Mo	V	Nb
Specimen of tee pipe	0.16	0.36	1.34	0.013	0.005	0.032	0.075	0.11	0.041	0.005	0.021
American standard ASTM A234 steel (Gr. WPR) [11]	≤0.20	Not required	0.40–1.06	≤0.045	≤0.045	Not required	1.60–2.24	0.75–1.25	Not required	≤0.05	≤0.02
Specimen of joint flange	0.22	0.27	0.84	0.014	<0.005	0.071	0.15	0.29	0.40	0.005	0.002
American standard ASTM A105 steel [12]	≤0.35	0.10–0.55	0.60–1.05	≤0.055	≤0.040	≤0.50	≤0.05	≤0.50	≤0.22	≤0.05	0.40

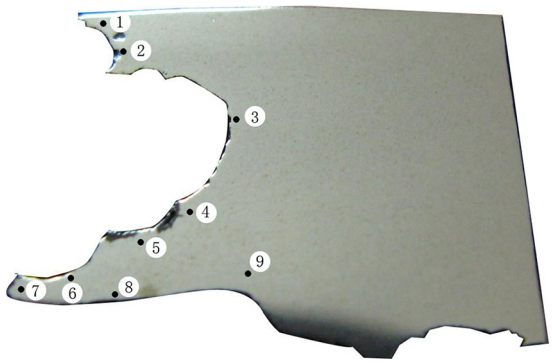

Fig. 2. Metallographic-grinding surface appearance of location A.

3.2.3. *Metallographic examination*

The specimens used for metallurgical examination are taken from locations A, B and C, as shown in Fig. 1. Location A is near the perforation and appeared to have a severely metallographically ground appearance, as shown in Fig. 2. The metallographic structure at location ⑨ is shown in Fig. 3, in which (b) is a partially enlarged image of (a); the metallographic structure is shown to primarily contain ferrite. As shown in the proportion of pearlite, the carbon content of the three-way

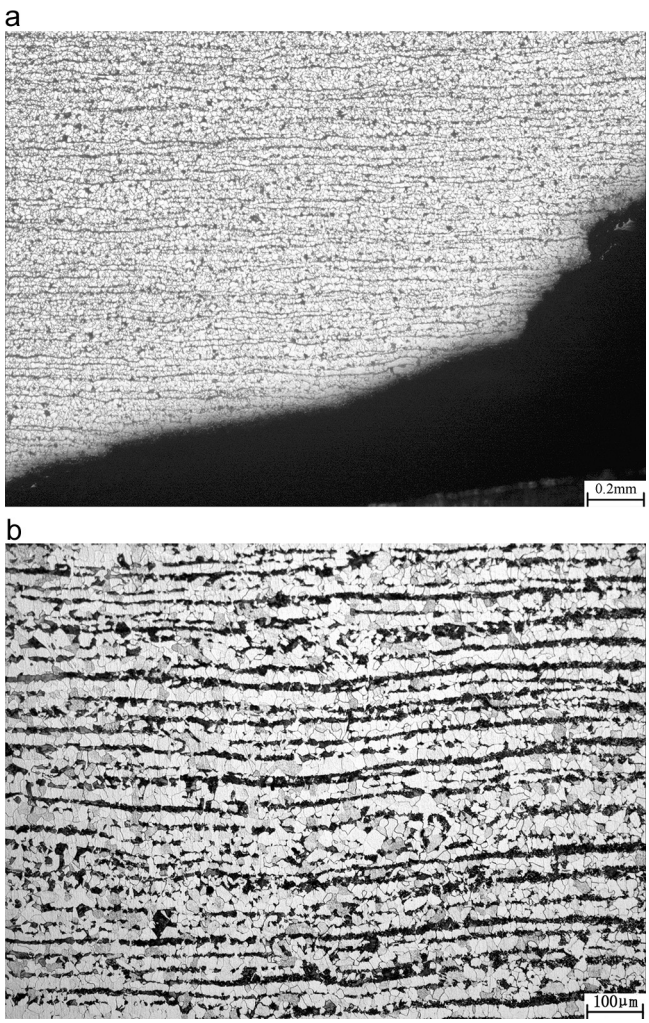

Fig. 3. Microstructure of location ⑨ in Fig. 2. (a) 50×; (b) 100×.

pipe material is 0.15–0.20%. At low magnification, the banded pearlite structures appear parallel to one another with each appearing similar to a straight line and nearly having the same width.

The metallographic structure denoted by locations ① through ⑧ in Fig. 2 is representative of the surface or sub-skin layer of the corroded cavity.

Location ① lies at the edge of the penetrating puncture and near the next external surface of the pipe (i.e., the bottom of the above-mentioned basin whose metallographic structure is shown in Fig. 4), where (b) is a partially enlarged image of (a), where a deformed streamline structure is shown. A deformed streamline structure is characterized by nearly parallel bands without external forces and deformations, as shown in Fig. 3. The distances between the pearlites are approximately equal; however, the pearlite bands are not parallel to one another and are disorganized.

A deformed streamline structure is shown near the surface or sub-surface of the corrosion-perforated hole, which indicates external forces acted on the area because general chemical corrosion and electrochemical corrosion do not cause deformed streamlines.

The characteristics of the metallographic structure are denoted by location ④ in Fig. 5, where (b) is a partially enlarged image of (a), and the characteristics at the edge of the corroded cavity are different from those denoted by locations ① and ②; the deformed streamline structures are not apparent, and the pearlite bands extend in parallel to the edge of the corroded cavity; also, the edge of the corroded cavity is not smooth, and the closed angles of it connect with the pearlite bands, which has the features of electrochemical corrosion. This occurred most likely because pearlite is a mixed two-phase structure that is easily corroded; also, although deformed streamline structures are not present, thin strips in the twin crystal can be observed in the ferrite phase, as indicated by the arrow in (b) [13]. These thin strips in the twin crystal have been observed on the other edge area as well. It is believed that the twin crystals formed due to deformation [14–18].

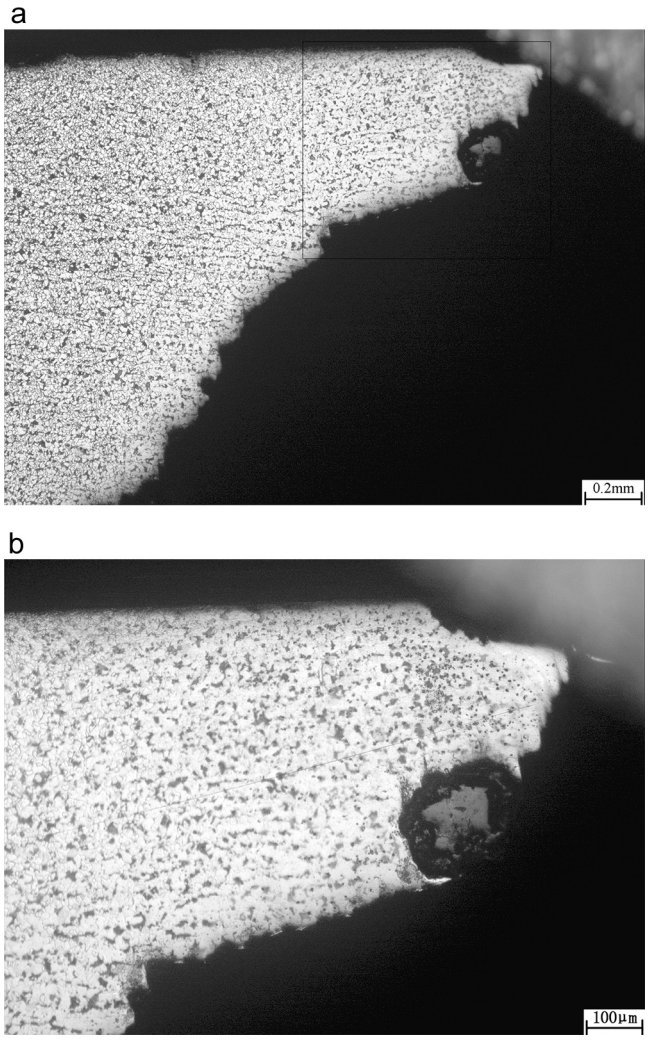

Fig. 4. Microstructure of location ① in Fig. 2. (a) 50×; (b) 100×.

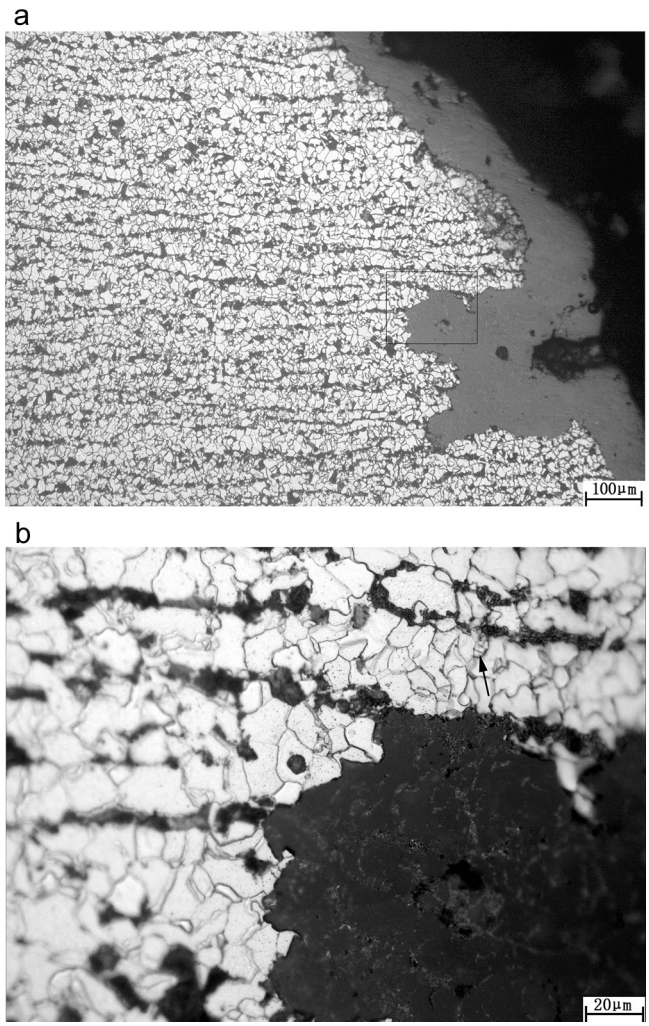

Fig. 5. Microstructure at location ④ in Fig. 2. (a) 50×; (b) 100×.

It is shown in Fig. 5 that corrosion began as electrochemical corrosion of the pearlite and then continued as external corrosion with applied force, as indicated by the presence of the twin crystals. If a large trench is first formed by alternative electrochemical corrosion, ferrite is separated into a "peninsula". When there is bubble burst, impact waves are typically generated, causing this "peninsula" to detach or simply further corrode electrochemically, isolating this "peninsula" and eventually causing it to break off.

As shown in Fig. 1(d), the macro-features of the corroded area were dominated first by electrochemical corrosion and then by turbulent flows. Cavitation erosion is indicated by the honeycomb-like appearance of the material. It is known that the fluids at the turn of the three-way pipe can easily reach a turbulent flow state, which is always accompanied by cavitations.

Due to the presence of surface or sub-surface deformation, deformation hardening should have occurred. The micro-hardness tests at locations ① and ② in Fig. 2 show that the hardness from the surface to the inside of the corroded cavity decreases from $163HV_{0.2}$ to $130–140HV_{0.2}$; this shows that the hardness of the surface and sub-surface increased due to deformation hardening.

All of these findings confirm that the surface or sub-surface of the corroded cavity was acted on by external forces, which originate from bubbles frequently appearing in the operating media, from the impact waves caused by the collapse of these bubbles (i.e., cavitation erosion [19]) and from scour caused by turbulent flow.

Fig. 5 also shows that the primary form of corrosion was electrochemical.

3.3. Characteristics of welded seam corrosion

The corroded cavity of the welded seam connecting the tee pipe and joint flange is indicated by arrow 5 in Fig. 1(b). The pattern of the cavity is shown in Fig. 6(a) and (b) shows the appearance of the corroded cavity of the welded seam at location "H" in (a) after metallographic grinding.

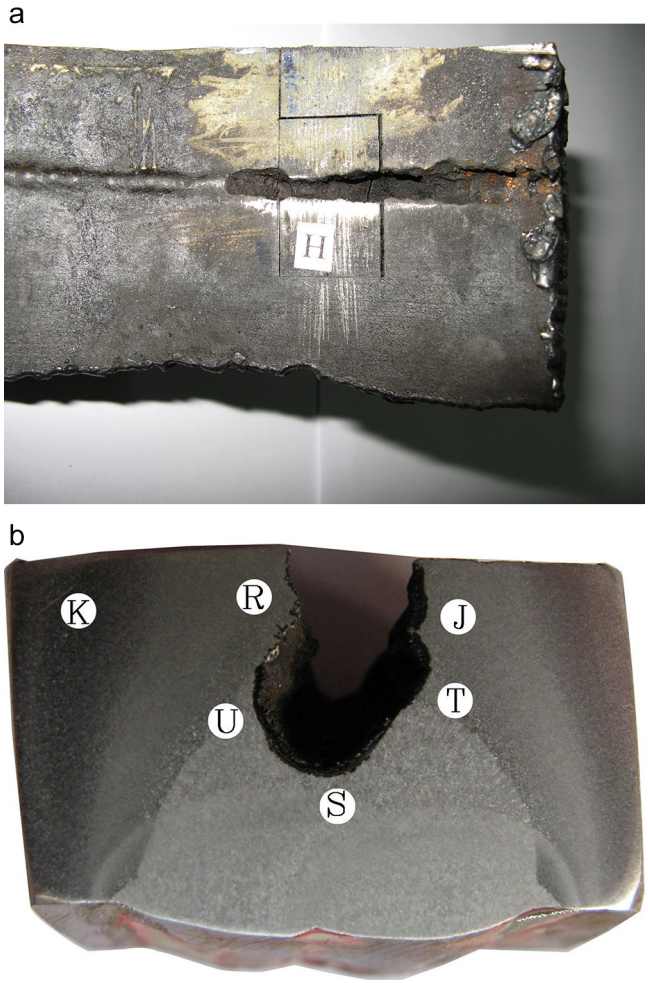

Fig. 6. Appearance of the corroded cavity of the welded seam. (a) pattern of the corroded cavity; (b) appearance of the cavity after metallographic grinding.

It can be seen from Fig. 6 that the welded seam is seriously corroded along its length and depth. Fig. 6(b) clearly shows the heat-affected area and basin appearance, which is shaped like a triangle. The area indicated by symbols Ⓡ, Ⓤ, Ⓢ, Ⓣ and Ⓙ is the corroded cavity in the range of the corroded basin.

Fig. 7 shows the metallographic structure of the molten pool of the welded seam, which is relatively complex and appears to have been caused by alternative electrochemical corrosion with features inside the columnar crystal that were corroded

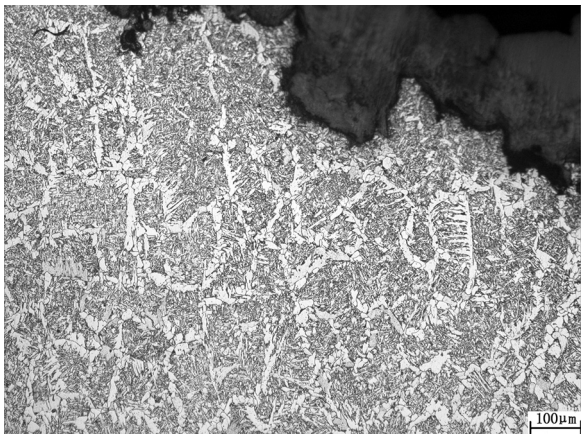

Fig. 7. Metallographic structure of the molten pool in the weld on the internal surface of the tee pipe.

first followed by its boundary. The columnar crystal is a multi-phase structure that can be rapidly corroded, while the boundary of the crystal is a single-phase ferrite, which is a feather-like carbon-free upper bainite, which corrodes slowly.

The front end (i.e., edge) of the corroded cavity shows that the corrosion extends in the direction of the columnar crystal; thus, the molten pool, whose front end is located at Ⓢ, is corroded more rapidly than locations Ⓡ and Ⓙ, and eventually forms a deep trench along the welded seam.

3.4. Analyses of electro-micrographic appearance

The tested specimen was taken from location "B" shown in Fig. 1(c) and was thoroughly washed clean in a physical way. A Japan-made electron detector EMPA-1600 was then used to characterize the surface appearance of the corroded cavity via secondary electrons, and the information of the related compositions is analyzed via X-ray energy-spectrum analysis.

Fig. 1(c) shows a large corroded cavity at location "B." which is the thinnest part of the cavity on the inner surface of the three-way pipe; the front edge of "B" is at the penetrating puncture.

Location "B" in Fig. 8 shows an electronic microimage obtained via secondary electron observation. It is seen from Fig. 8(a) that the surface of the corroded cavity appears similar to the beach marks formed by the regular arrangement of small pits. The range of the corroded cavity is divided into several areas, whose small pits are consistent in their arrangement directions. However, the arrangement directions of the small pits in different areas vary; certain areas appear like "farmland," as shown in Fig. 1(b) and (c), while the boundary between two areas appear like "ridges."

The image shown in Fig. 8(b) shows features that can only be caused by mechanical actions with the fracture mode similar to those of quasi-cleavage fractures. As mentioned above, the corrosion caused by bubbles breaking and from the scour of the turbulent flow is the result of material peeling off layer by layer. Whenever a layer peels off, new fractures begin, leading to secondary cracks that can be clearly seen along the direction of the crystals. Metallographic inspection of the axial ground

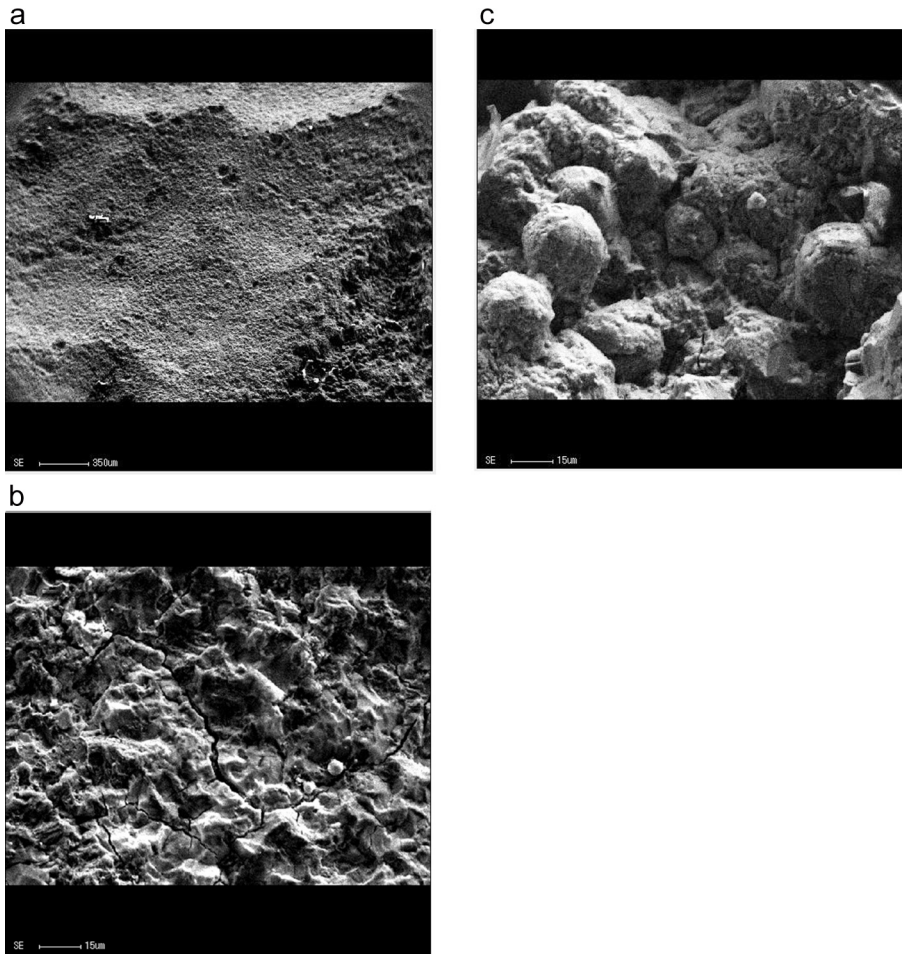

Fig. 8. Electronic micro-image of location "B". (a) Surface of the corroded cavity; (b) amplified image of the corroded cavity; and (c) amplified image of the corroded cavity in another area.

surface of the pipe ruled out the possibility of intercrystalline corrosion. It is quite certain that the cracks along the direction of the crystals were caused by the process of layers peeling off and thus mechanical action.

The image shown in Fig. 8(c) reveals the cellular structure, secondary cracks along the direction of crystals and the features of the chemical corrosion observed.

3.5. X-ray energy-spectrum microinspection of related compositions of large corroded cavities on the inner surface of the tee pipe

To confirm the chemical compositions of the materials of the corroded area on the surface of the inner wall of the tee pipe, X-ray energy-spectrum microinspection of chemical compositions was performed. Location "A" in Fig. 1(c) shows the inspected area near to the penetrating puncture. The tested results show that the corroded surface contains large concentrations of oxygen, carbon, and nitrogen with smaller concentrations of sulfur, chlorine, silicon, sodium, magnesium, aluminum, potassium, titanium, etc., all of which are corrosion products caused by sea water.

The spectrum bands of the chemical compositions of materials at location "A" are shown in Fig. 9.

4. Discussion

Cavitation corrosion is a special form of erosion corrosion. When a liquid flow is dropped below its critical steam pressure, precipitation of dissolved gases in the liquid will occur, forming bubbles and increasing the volume of the fluid; this process called

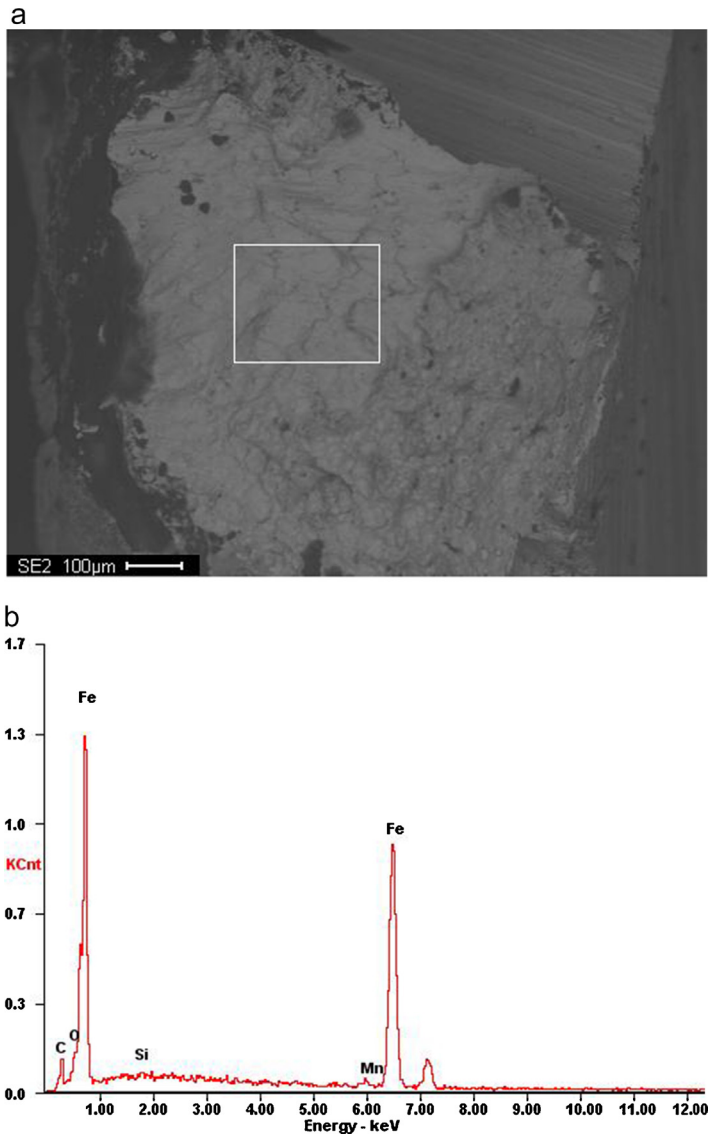

Fig. 9. X-ray energy spectrum on the surface at location "A". (a) analysis region; and (b) spectrum line of chemical compositions in the micro-regions.

cavitation. As a result, the fluid pressure increases, and the bubbles are compressed until they collapse. The mechanism produces damaging effects on surrounding structures when the bubbles collapse due primarily to shock waves, as described by Rayleigh theory and the liquid microjet Kornfeld theory. Shock wave theory states that the bubble collapse process will radiate a spherical shock wave and have a direct effect on material surfaces, causing damage. Micro-jet theory states that liquid micro-jets reach speeds up to 100 m/s and are caused by bubbles bursting; the collapse pressure is near 10^8 MPa, and the impingement area is small, resulting in high stresses and thus material damage. Because cavitation erosion is related to the fields of hydrodynamics, thermodynamics, bubble dynamics, and materials mechanics, an accepted theory has not yet been formed.

It was found through the failures of heat exchangers that impingement attack (i.e., erosion corrosion) occurs where gases, vapors or liquids impinge on metal surfaces at high velocities. The erosive action removes protective films from localized areas at the metal surface, contributing to the formation of differential cells and localized pitting of anodic areas. Impingement attack usually produces a horseshoe-shape pit [20,21]. Evidently, both cavitation and liquid impingement exert similar hydrodynamic forces on a solid surface. Frederick G.H. and Frank J.H. believed that the appearance of damaged surfaces and the relative resistance of materials to damage are similar for both liquid-impingement and cavitation erosion [22]. Thus, cavitation erosion usually produces a horseshoe-shape pit.

Additionally, corrosion was once thought to play an essential role in cavitation erosion, but recent experiments (most notably, tests of plastics in water and of aluminum in toluene) strongly indicate that damage can occur even without corrosion. This does not mean that corrosion does not cause damage in situations where corrosion is known to occur, but rather that corrosion is not a necessary factor to produce damage [23].

Based on the above analysis of corrosion phenomena and corrosion morphology, the penetration of the tee pipe was caused by cavitation erosion. On the surfaces and sub-surfaces of the large corroded cavities, the depths of which ranged from 1 μm and 10 μm, the shapes of which are like a horse's hooves or polygons, and the boundaries of which are smooth, there are deformation lines and twin crystals contained in the ferrite phases. All results indicate that the corrosion is characterized by cavitation erosion [21].

The pipe wall was found to have peeled off and thinned due to mechanical action until it was perforated; this process can be described as follows. The significant impacts from cavitation shock waves made the surface or sub-surface of the pipe deform, forming one cavity or several cavities, from which some metal was removed and piled up at the edge of the pit, forming a "ridge" after many cycles, as shown in Fig. 8(a) and (b). The shock waves resulting from cavitation increased shear stress, which can also be produced by turbulent flows and tends to damage the "ridge" formed; thus, a layer of the pit could be removed, depending on whether the impact waves were small or large. The cracks on the surface or sub-surface made it easy for the skin layer to peel off. Because oil-containing sewage is a corrosive medium, cavitation erosion of the tee pipe was accompanied by chemical/electrochemical corrosion. When the old surface peeled off to reveal a new high-activity surface, which is even more easily corroded, the surface of the pipe was continuously corroded and peeled off layer by layer when bubbles impinged on the etched surface.

5. Conclusions

The material of the tee pipe is required to be the steel specified in the American standard ATSM (i.e., Gr. WPR, ASTM234). However, the inspected results of the chemical compositions of the corroded parts show that the Cu and Ni contents are very low and do not meet the quality standards. However, the chemical composition of the material of the joint flange meets the requirement of A105 steel specified in the American standard ASTM except the content of Nb.

The configuration of the large corroded pit appears like an imperfect "horse's hoof", and its interior is completely corroded, forming a honeycomb-like cavity. Characteristics of cavitation erosion and turbulence erosion are found.

Deformed streamline structures or twin crystals in the ferrite phase and the change in micro-hardness near the surface or sub-surface of the penetrating puncture are all strong indications of cavitation erosion.

The penetrating puncture at the turn of the tee pipe was likely caused by cavitation erosion accompanied by chemical/electrochemical corrosion. The serious corrosion of the seam connecting the tee pipe and the flange was primarily the result of electrochemical corrosion.

6. Suggestions

To improve the corrosion resistance of a material, it is beneficial to first guarantee a proper yield ratio and then to increase the material strength. Provided that the steel has the correct Cr content, its cavitation erosion resistance can be improved.

To reduce the possibility of bubble production and accumulation, to reduce the content of air contained in the operating fluid and to reduce the flow speed of the fluid, it is necessary to regularly wash out pipes with a pressurized fluid to remove corrosion products.

To lessen the influence exerted by turbulent flow, it is essential to improve the design and manufacturing technique of the bend at the turn of the tee pipe.

References

[1] Abedi SSh, Abdolmaleki A, Adibi N. Failure analysis of SCC and SRB induced cracking of a transmission oil products pipeline. Eng Fail Anal 2007;14(1):250–61.

[2] Shalaby HM, Riad WT, Alhazza AA, Behbehani MH. Failure analysis of fuel supply pipeline. Eng Fail Anal 2006;13:789–96.
[3] Azevedo CRF. Failure analysis of a crude oil pipeline. Eng Fail Anal 2007;14:978–94.
[4] Peng C-h, Liu Z-y, Wei X-z. Failure analysis of a steel tube joint perforated by corrosion in a well-drilling pipe. Eng Fail Anal 2012;25:13–28.
[5] Lin M-B, Gao K, Wang C-J, Volinsky AA. Failure analysis of the oil transport spiral welded pipe. Eng Fail Anal 2012;25:169–74.
[6] Shahriar A, Sadiq R, Tesfamariam S. Risk analysis for oil and gas pipelines: a sustainability assessment approach using fuzzy based bow-tie analysis. J Loss Prev Process Ind 2012;25(3):505–23.
[7] Rauf A, Mahdi E. Surface damage caused by erosion-enhanced pitting corrosion of API-X52 steel used as oil and gas transportation pipeline material. In: Proceedings of the 3rd Gas Processing Symposium; 2012. p. 311–8.
[8] The Materials Information Company. Metals handbook. 9th ed. Failure analyses and prevention, vol. 11, 9th ed. 2002;p. 2174.
[9] Winston Revie R. Uhlig's corrosion handbook. 2nd ed. New York: John Wiley & Sons, Inc.; 2000. p. 249–69.
[10] Bianchi G, Fiori G, Longhi P, Mazza F. Horse Shoe corrosion of copper alloys in flowing sea water: mechanism, and possibility of cathodic protection of condenser tubes in power stations. Corrosion 1978;34(1):396–406.
[11] American society for Testing and Materials (ASTM). A234/A 234M-02, Standard specification for piping fittings of wrought carbon steel and alloy steel for moderate and high temperature service. West Conshohocken, PA, United States: ASTM International; 2002.
[12] American society for Testing and Materials (ASTM). ASTM A105/A105M-05, Standard specification for carbon steel forgings for piping application. West Conshohocken, PA, United States: ASTM International; 2005.
[13] Xie J, Fu H, Zhang Z, Jiang Y. Deformation twinning feature and its effects on significant enhancement of tensile ductility in columnar-grained Fe–6.5 wt.%Si alloy at intermediate temperatures. Intermetallics 2012;23:20–6.
[14] Johnson JN, Rohde RW. Dynamic deformation twinning in shock-loaded iron. J Appl Phys 1971;42:4171.
[15] Altshuler TL, Christian JW. Low temperature twinning in pure iron. Acta Metall 1966;14(7):903–8.
[16] Sleeswyk AW. Emissary dislocations: theory and experiments on the propagation of deformation twins in α-iron. Acta Metall 1962;10(8):705–25.
[17] Wasilewski RJ. Coherent (1 1 0) boundaries of b.c.c. twins. Acta Metall 1966;14(12):1870–1.
[18] Hamer FM, Hüll D. Nucleation of twinning and fracture. Acta Metall 1964;12(5):682–4.
[19] Haosheng C, Shihan L. Inelastic damages by stress wave on steel surface at the incubation stage of vibration cavitation erosion. Wear 2009;266(1–2):69–75.
[20] Boyer HE. Metals handbook. 8th ed. Failure analysis and prevention, vol. 10, 8th ed. Metals Park: American Society for Metals; 1974. p. 551.
[21] Winston Revie R. Uhlig's corrosion handbook. 2nd ed. New York: John Wiley & Sons, Inc.; 2000.
[22] Boyer HE. Metals handbook. 8th ed. Failure analysis and prevention, vol. 10, 8th ed. Metals Park: American Society for Metals; 1974. p. 161.
[23] Boyer HE. Metals handbook. 8th ed. Failure analysis and prevention, vol. 10, 8th ed. Metals Park: American Society for Metals; 1974. p. 162–3.